Materials Chemistry and Physics 129 (2011) 910–918

Contents lists available at ScienceDirect

Materials Chemistry and Physics

journal homepage: www.elsevier.com/locate/matchemphys

Synthesis and characterization of xMgO–1.5Al_2O_3–5SiO_2 (x = 2.6–3.0) system using mainly talc and kaolin through the glass route

Johar Banjuraizah [a], Hasmaliza Mohamad [b], Zainal Arifin Ahmad [b,*]

[a] School of Materials Engineering, Universiti Malaysia Perlis, 02600 Kangar, Perlis, Malaysia
[b] School of Materials and Mineral Resources Engineering, Universiti Sains Malaysia, Engineering Campus, 14300 Nibong Tebal, Penang, Malaysia

ARTICLE INFO

Article history:
Received 25 October 2010
Received in revised form 23 February 2011
Accepted 13 May 2011

Keywords:
A. Glasses
B. Crystallization
C. Powder diffraction
D. Thermal properties
D. Dielectric properties

ABSTRACT

Three non-stoichiometric cordierite with compositions of xMgO–1.5Al_2O_3–5SiO_2 (x = 2.6–3.0 mol) were synthesized using mainly talc and kaolin through the glass route. The densification and crystallization behaviors of these glass powders were investigated using DTA, dilatometer, and XRD. Samples were then heat treated at 900 °C for 2 h and further analyzed using XRD, CTE, FESEM, density and porosity tests, and also dielectric test to further investigate their properties. The 2.8MgO·1.5Al_2O_3·5SiO_2 glass composition fully densified and crystallized into high purity α-cordierite at the heat treatment temperature. It exhibited lower CTE and dielectric constant compared to other composition, making it suitable for high frequency applications. Other formulations which contain multi crystalline phases require much higher temperatures for densification. The CTE value depends on the type of crystalline phase which exist in the sample, while the dielectric constant decreased with increasing MgO amounts in the sample compositions.

1. Introduction

α-Cordierite-based glass–ceramics have attracted some attention in recent years owing to their low CTE, dielectric constant, dielectric loss and density which make them suitable for high frequency applications. The difficulty of obtaining high crystallinity α-cordierite phase at or below 900 °C with a short soaking time using solid state [1–5] and sol–gel [6–9] methods can be reviewed in the literature. Although it has been reported that α-cordierite can be crystallized at 900 °C using the glass route [10], the crystallization of secondary crystalline phases, together with large amorphous phases, will significantly affect its properties. Furthermore, the crystallization that occurs before the densification process would cause the viscosity of the glass to increase, resulting in higher porosity of glass–ceramics. This problem can be overcome by reducing the softening temperature and viscosity of the glass. Besides the addition of sintering aids and pulverizing into very fine particles, the viscosity of the glass can be further reduced by modifying the stoichiometric compositions.

Previously, we reported the effects of excess MgO concentration from cordierite stoichiometric compositions on phase transformation which is in the series of xMgO·2Al_2O_3·5SiO_2 (where x = 2–4 mol) [11], and also the densification and crystallization behavior of these compositions [12]. Although compositions with high MgO concentrations had enhanced the crystallization of the α-cordierite phase, small amounts of spinel ($MgAl_2O_4$) and forsterite also tended to crystallize [11]. Additionally, it has been proven from these studies that excess MgO in a stoichiometric cordierite composition would not only cause the densification temperature to decrease, but also the crystallization temperature [12]. In fact, some of the studied compositions tend to crystallize before densification has completed. Crystallization that occurs before densification may have been initiated from insufficient melting temperature used to melt the glass compound or a low quenching rate. This will cause small amounts of glass to crystallize during melting and consequently retards the viscous sintering process during heat treatment of the glass. McMillan [13] in his book proposed that the melting temperature of the glass compound can be reduced by reducing the intermediate oxide of the glass, which is Al_2O_3 in this system, and this will consequently decrease the viscosity of the glass if the same melting temperature was employed. In addition to that, a reduction in Al_2O_3 mole ratio is expected to retard the formation of spinel as excess MgO will react with Al_2O_3 to form spinel ($MgAl_2O_4$), while variations in MgO concentrations will retard the formation of forsterite. Therefore, by systematically modifying the compositions of study, the crystallization of the intended phase can be controlled by impeding the reaction and crystallization of the secondary phase. Although it has also been reported in the literature [14–18] that the MAS composition used with excess MgO and less Al_2O_3 would contribute to better densification and crys-

* Corresponding author. Tel.: +60 4 5996128; fax: +60 4 5941011.
E-mail address: zainal@eng.usm.my (Z.A. Ahmad).

0254-0584/$ – see front matter © 2011 Elsevier B.V. All rights reserved.
doi:10.1016/j.matchemphys.2011.05.026

Table 1
Elemental analysis of minerals and oxide compound by XRF.

	Kaolin	Talc	SiO_2	Al_2O_3	MgO
	wt%				
MgO	0.88	49	–	–	99
SiO_2	59	47	99.5	0.2	–
Al_2O_3	35	0.16	0.04	99.46	–
K_2O	3	–	–	–	–
CaO	0.014	3	–	0.075	0.13
TiO_2	0.84	–	–	–	–
Fe_2O_3	0.6	0.45	0.04	0.15	0.0036
Cr_2O_3	0.032	–	–	–	–
NiO	0.014	0.028	–	0.022	–
P_2O_5	0.073	0.095	–	–	–
ZrO_2	0.05	–	–	–	–
SO_3	–	0.06	–	–	0.07
CuO	–	0.016	–	0.014	–

Table 2
Composition of oxides in the mixtures.

Sample	MAS ratio	MgO (g)	Al_2O_3 (g)	SiO_2 (g)
X1	3:1.5:5	21.0548	26.6322	52.3131
X2	2.8:1.5:5	19.9309	27.0113	53.0578
X3	2.6:1.5:5	18.7745	27.4014	53.8241

tallization behavior, it must be noted that pure oxides were used as their initial raw materials and the compositions were different from the one used in the present study.

Therefore, besides the use of compositions with excess MgO concentration in this present study, mole of intermediate oxide was also reduced. Al_2O_3 was reduced to 1.5 mole ratio, while SiO_2 mole ratio was kept constant at 5 moles as the exact cordierite stoichiometric composition for all investigated compositions. The effect of MgO concentration in a series of xMgO·1.5Al_2O_3·5SiO_2 samples was examined. The compositions of the present research were systematically chosen based on previous studies so as to increase the purity of the α-cordierite phase as well its densification behavior.

2. Materials and methods

MgO–Al_2O_3–SiO_2 glass–ceramics with different mole ratios were synthesized using kaolin (Kaolin Industry, Tapah Perak, Malaysia) and talc (Ipoh Ceramic, Sdn Bhd, Ipoh Malaysia). Silica (Ipoh Ceramic, Sdn Bhd. Ipoh, Malaysia), alumina (Metco, Westbury, USA) and magnesia (Merck, Whitehouse Station, NJ) were added to compensate the formulation of the compositions. The amount of talc and kaolin used in each composition studied was weighted to the optimum amounts in order to minimize the use of pure metal oxides. The elemental composition of the initial raw materials was determined by X-ray florescence spectroscopy (Rigaku X-Ray Spectrometer model RIX 3000) and the details are given in Table 1. Tables 2 and 3 summarize the detailed compositions of oxide and the weight percent of initial raw materials. The homogenized mixtures of raw ingredients were melted in alumina crucibles at 1500 °C for 4 h in air. Frits were produced by quenching the melts in distilled water, and were dry milled using Pulverized 6 to obtain fine glass powders with average of particle sizes in the range of 1–3 μm.

Two sets of DTA analyses were carried out. The first data was collected from the glass powder heated at 5 °C min^{-1} from room temperature up to 900 °C and was kept isothermally at 900 °C for 1 h (Model Linseis). The second DTA was collected from the sample non-isothermally heated from room temperature to 1000 °C at 5 °C min^{-1} heating rate. Rectangular specimens (5 mm × 3 mm × 20 mm) for the dilatometry test were prepared by compaction of the glass powder using a Hydrotex uniaxial pressing machine at 120 MPa. Sintering reactions at increasing temperatures were tested using a dilatometry test with a high temperature vertical dilatometer (Model Linseis) from room temperature to 1100 °C. The X-ray diffraction (XRD) patterns of the glass powders and sintered products were obtained using a Bruker D8 Advanced operated in Bragg–Brentano geometry, with Cu Kα radiation. Counting time was fixed at 71.5 s for each 0.03°2θ step. The X-ray tube was operated at 40 kV and 30 mA. All XRD instrument parameters set up were fixed to standard value during the measurements. Bulk density and apparent porosity were measured by Archimedes immersion technique. Microstructures of the fractured samples were observed using a field emission scanning electron microscopy (VP FESEM-Supra 35VP) at 30 kV. Specimens for the CTE and dielectric test were prepared by compaction of the glass powder using a Hydrotex uniaxial pressing machine at 120 MPa. The samples were sintered in air under isothermal conditions for 2 h at 900 °C with a 5 °C min^{-1} heating rate before CTE and dielectric testing. The CTE test was carried out using high temperature vertical dilatometer tests (Model Linseis) in air from room temperature to 1200 °C, while the dielectric measurements were made using an Impedance Analyzer (Hewlet Packard model HP4291). The specimens were ground and polished down to a 1 μm diamond paste, washed in water and acetone and heated at 100 °C for 2 h to remove moisture prior to the dielectric measurement. The results of dielectric constant and dielectric loss as a function of frequency can be obtained directly when the sample thickness is fed into the machine.

Table 3
Composition of initial sample based minerals.

Sample	MAS ratio	Talc (g)	Kaolinite (g)	MgO (g)	Al_2O_3 (g)	SiO_2 (g)
X1	3:1.5:5	30.0000	64.0000	6.3550	4.2320	0.4531
X2	2.8:1.5:5	31.0000	65.0000	4.7400	4.2600	0.1400
X3	2.6:1.5:5	31.0000	65.0000	3.5845	4.6514	0.9040

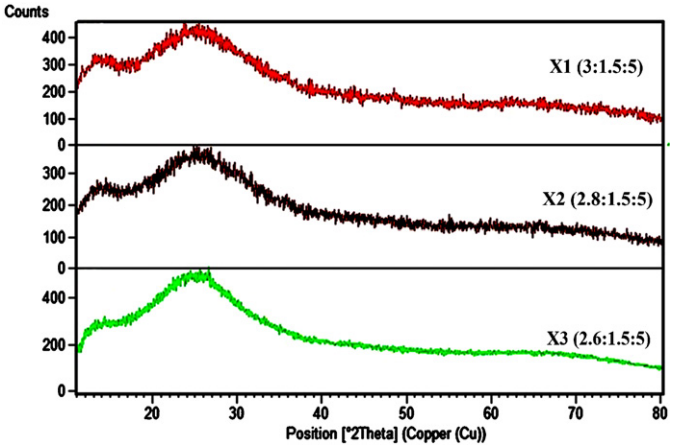

Fig. 1. XRD pattern of glass powder for samples X1, X2 and X3.

3. Results and discussion

3.1. XRD pattern of glass powder

Fig. 1 shows a large amorphous hump and no crystalline peaks in the diffraction patterns for the all three glass powder samples. This indicates that all compounds in the samples have transformed into amorphous or glassy phase after being melted at 1500 °C for 4 h. Reduction of intermediate oxide (Al_2O_3) in the glass compositions was proven to be able to reduce the melting temperature as well as the viscosity of the glass at 1500 °C causing no crystalline phase to appear in the diffraction pattern of milled glass powder.

3.2. Non-isothermal and isothermal DTA analysis

Fig. 2 demonstrates the DTA scan of the glass sample in a non-isothermal condition. Only a single exothermic peak was present in each sample. The weak exothermic peak belongs to sample X3 with composition 2.6MgO·1.5Al_2O_3·5SiO_2 which has the least MgO concentration among the three studied samples. The position of the crystallization peak also varies with compositions. The increase of MgO concentration caused a shift of the crystallization peak maxima to lower temperatures. The crystallization temperature decreased from 925 °C to 876 °C for samples with 2.6–3.0 MgO concentration as given in Fig. 3. This result was in agreement with experiments conducted using a series of samples with the formulation xMgO·2Al_2O_3·5SiO_2 [11]. DTA curves also indicate that the crystallization peak becomes more intense, and the area under the DTA peak becomes larger with increasing amounts of MgO, as demonstrated in Fig. 4.

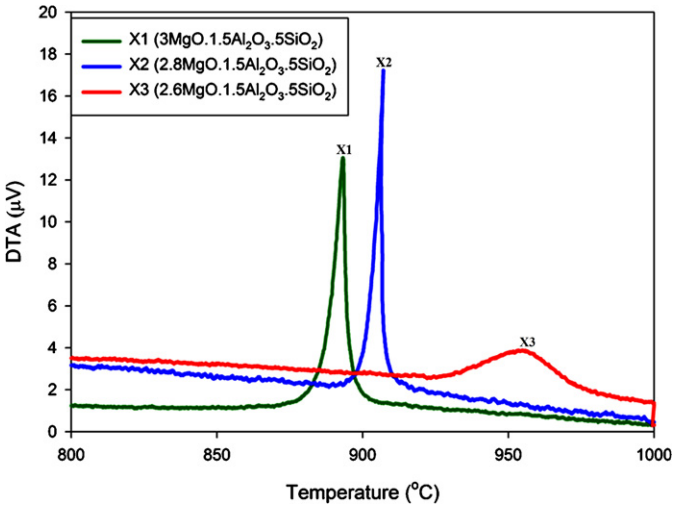

Fig. 2. Nonisothermal DTA curves of samples with various MAS ratios.

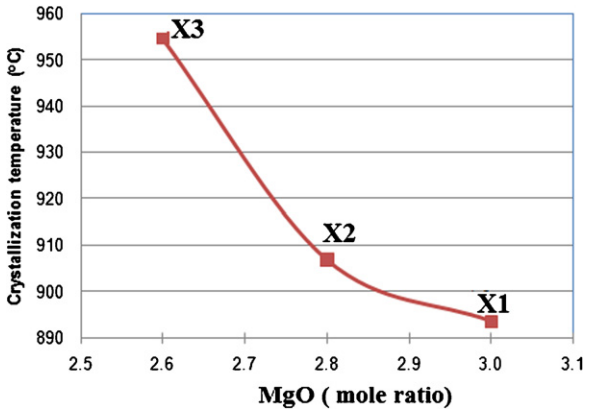

Fig. 3. Crystallization temperature for samples with increasing MgO concentration for series xMgO·1.5Al_2O_3·5SiO_2.

Although the nonisothermal DTA curve in Fig. 2 shows that the crystallization range of samples X1 and X2 ended above 900 °C, prolonged soaking for 2 h would be beneficial to improve the crystallization process at intended heat treatment temperatures, as demonstrated in Fig. 5. As shown in Fig. 5 complete exothermic peaks were observed for samples X1 and X2 in the isothermal DTA curve during heating at 900 °C for 2 h. However, no exothermic peak was observed for sample X3 with composition 2.6MgO·1.5Al_2O_3·5SiO_2. Although the XRD pattern from compacted glass specimen of sample X3 demonstrated that the crystalline peak appeared after prolonged sintering for 2 h at 900 °C, the intensity of the peaks are lower compared to the other two samples. It was expected for surface crystallization to have occurred in this compacted and sintered sample since no exothermic peak was present in the DTA curve of the same glass powder sample heated at the same heat treatment parameters. The crystallization of μ-cordierite or magnesium dialuminum silicate phase in sample X3 after heat treatment strongly indicates that the crystallization process is restricted to the glass surface [19,20]. The absence of the exothermic peak in the DTA curve was expected to have resulted from the lower driving force for surface crystallization of the loose glass powder sample (for DTA test) compared to compacted glass powder sample (for XRD test). Therefore, the numbers of crystals nucleated strongly depend on the chemical composition of the parent glass and do not depend on temperature and time of the heat treatment process [21].

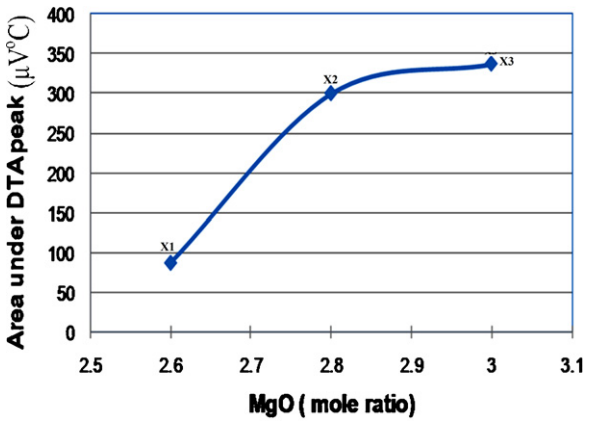

Fig. 4. Integrated area under nonisothermal DTA peaks.

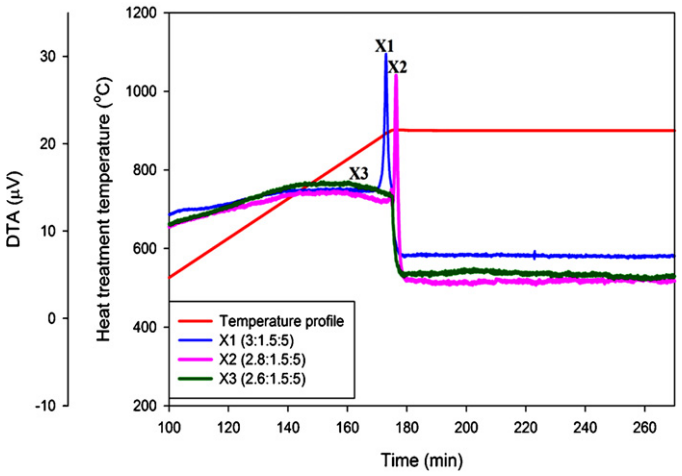

Fig. 5. Isothermal DTA plot for samples X1, X2 and X3.

3.3. Dilatometry curve

The dilatometry test was carried out on un-sintered samples to determine the sintering reaction curve as a function of temperature. The rectangular green samples were non-isothermally heated from room temperature to 1000 °C. Fig. 6 shows a typical dilatometric

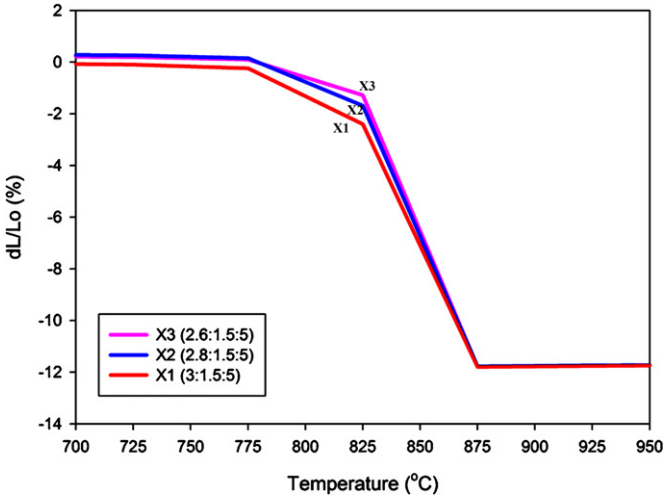

Fig. 6. Dilatometry curve of unsintered compacted glass powder.

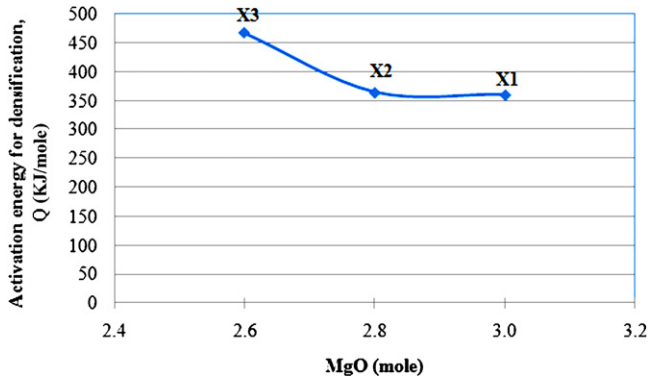

Fig. 7. Activation energy for densification of glass sample with composition xMgO·1.5Al_2O_3·5SiO_2.

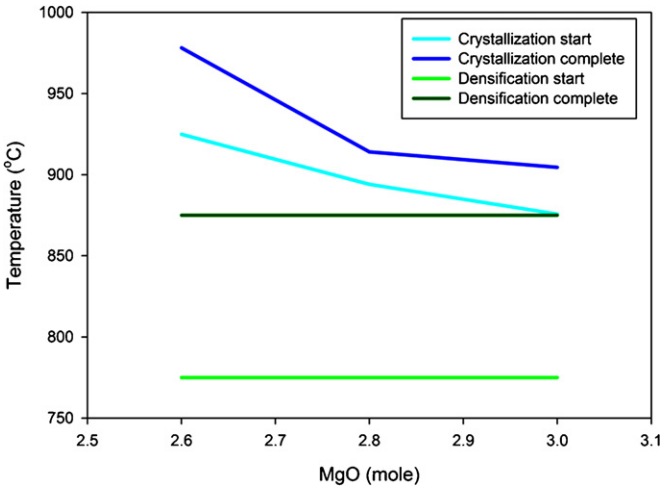

Fig. 8. Densification and crystallization temperature of samples with various MAS ratios.

curve for un-sintered samples with different MgO concentrations. It can be seen that the expansion values for all samples with different MgO concentrations are very close to each other at the initial stage when heated from room temperature up to 775 °C and accelerated at 825 °C. At this temperature range, the viscosity of the glass is dramatically decreased. All samples stop obvious shrinking approximately at 875 °C with a similar percentage of shrinkage (12%). Because of the surface tension effect that varies as a function of surface curvature, material flows are driven toward the particle necks, thus densifying a glass powder compact.

Although the softening and final shrinkage temperatures were the same for all three samples, the shrinkage rate of the three samples was different as a function of temperature. This can be observed through the slope at the shrinkage part. Based on the slope of the curves, sample X1 has a higher shrinkage rate followed by samples X2 and X3. The difference in shrinkage rate of samples is greatly related to the viscosity of glass. Glass with low viscosity easily flowed, causing samples with higher MgO concentrations to have higher shrinkage rates. Thus, varying the amount of MgO concentrations in non-stoichiometric cordierite composition with less intermediate oxides would also affect the viscosity of the glass.

3.4. Activation energy for densification

Activation energy for densification of glass powder samples with different compositions is shown in Fig. 7. The activation energy for densification Q was calculated when the sample experiences shrinkage (between 825 and 875 °C) from the dilatometry curve using the Arrhenius equation [12]. From the figure, the activation energy for densification tended to decrease with increasing MgO concentrations in the compositions. This result (in xMgO·1.5Al_2O_3·5SiO_2 series) was in good agreement with results obtained from previous studies in non-stoichiometric cordierite samples in xMgO·2Al_2O_3·5SiO_2 series where Q decreased with increasing MgO [12]. However, the activation energy for densification tends to plateau above 2.8 mol MgO.

Fig. 8 demonstrates plots of densification and crystallization temperature as a function of MgO. The range of crystallization temperature slightly decreased with increasing MgO concentration ratio, while the temperature range for densification is similar for all three samples which is below the range of crystallization temperature. This indicates that densification occurred before crystallization. The gap between densification and crystallization temperatures is high in sample X3 followed by samples X2 and X1, respectively. Although sample X1 has the lowest crystallization temperature among the three samples where crystallization may start below 900 °C, the crystallization process is difficult to control since the gap between densification and crystallization temperature is very close.

3.5. XRD analysis of sintered pellet

As shown in Fig. 9, four crystalline phases that were observed in these 3 samples are α-cordierite (ICSD 98-005-8888), forsterite (ICSD 98-008-5876), spinel (ICSD 98-005-8457), and μ-cordierite or magnesium dialuminium trisilicate (ICSD 98-000-770). Although no exothermal peak was observed in the isothermal DTA curve of sample X3 with composition 2.6MgO·1.5Al_2O_3·5SiO_2, results of XRD pattern on the sintered compacted pellet revealed the appearance of crystalline peaks in the diffraction pattern. Both glass powder (DTA test) and compacted glass powder (XRD) samples of the same composition experienced the same heat treatment profile, but pressed pellets, in contrast to loose powder samples, tend to crystallize during prolonged holding at the same heat treatment temperature. The diffusion and the arrangement of atoms for crystallization would be enhanced if the particles are very close as in compacted powders.

As demonstrated in the diffraction pattern, the main crystalline phase in sintered pellets for all three samples was α-cordierite. It can be clearly seen that the intensity of the α-cordierite peak

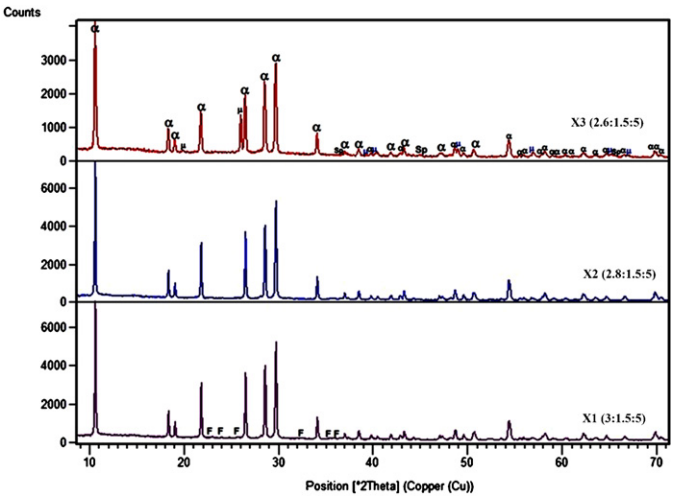

Fig. 9. X-ray diffraction patterns of samples with different MAS ratios sintered at 900 °C for 2 h (α: α-cordierite, f: forsterite, μ: μ-cordierite, sp: spinel).

Table 4
Results of Rietveld refinement.

Sample	Phases	Quantity (wt%)	R_{Bragg}	R_{wp}	S	R_{exp}	R_p
X1	Amorphous	2.30					
	α-Cordierite	89.20	12.35	11.31	2.78	6.78	9.19
	Forsterite	8.50	33.21				
X2	α-Cordierite	100.00	11.52	9.55	1.55	6.17	7.5 0
X3	Amorphous	46.20					
	α-Cordierite	45.78	17.54	11.50	3.21	6.41	9.00
	μ-Cordierite	7.59	2.59				
	Spinel	0.38					

R_{Bragg}: agreement indices on Bragg value; R_{wp}: agreement indices on the weighted value; S: goodness of fit; R_{exp}: agreement indices on expected value; R_p: agreement indices on the profile value.

became higher as the amount of MgO used was increased, and sample X3 with chemical formulation $2.6MgO{\cdot}1.5Al_2O_3{\cdot}5SiO_2$ had the lowest intensity compared to the other 2 samples. Small amounts of secondary phases were observed in samples X1 and X3. μ-Cordierite and spinel peaks appeared in sample X3, while the forsterite peak appeared in sample X1. Theses crystalline phases are normally present in crystallization of MAS glass [18,22]. The existence of these types of secondary phase in samples with 2.6 mol and 3 mol MgO is similar with the series of $xMgO{\cdot}2Al_2O_3{\cdot}5SiO_2$ samples [11]. Results of phase quantification are tabulated in Table 4.

Decreasing the amount of MgO retarded the formation of the forsterite phase, while decreasing the amount of Al_2O_3 from stoichiometric $2.8MgO{\cdot}2Al_2O_3{\cdot}5SiO_2$ successfully retarded the formation of the spinel phase. Single phase α-cordierite was observed in sample X2 with composition $2.8MgO{\cdot}1.5Al_2O_3{\cdot}5SiO_2$. A comparison of the intensity counts of α-cordierite at (0 2 2) plane also indicates that the intensity of the α-cordierite phase is higher in the sample with 2.8 mol of MgO, and the intensity counts for the three samples are parallel with the amount of α-cordierite phase present in the samples as shown in Fig. 10.

Fig. 11 shows one of the Rietveld plots of the XRD data for sample X3 which was heat treated at 900 °C for 2 h. The Rietveld plots show a good quality of refinement. The results are normalized to 100% of crystalline fraction, so the hyphothetical amorphous content of the sample was assumed to be negligible.

Percentage of the amorphous content was calculated using the Fullprofile pattern method. The results of the quantitative phase analysis, including the amorphous phase, are tabulated in Table 4. Sample X3 still contains a high amount of amorphous phase. As obtained in the non-isothermal DTA test, the crystallization temperature range of sample X3 is above 900 °C. Therefore, prolonged holding of the compacted pellet up to 2 h would not effectively transform the glass into a fully crystalline phase. This composition requires a much higher heat treatment temperature to enhance the crystallization process. Small amounts of amorphous phase were

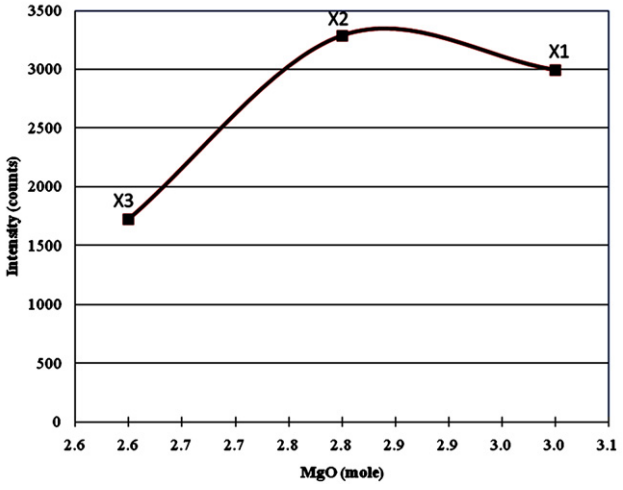

Fig. 10. Intensity of α-cordierite peak count at (0 2 2) plane as a function of MgO concentration.

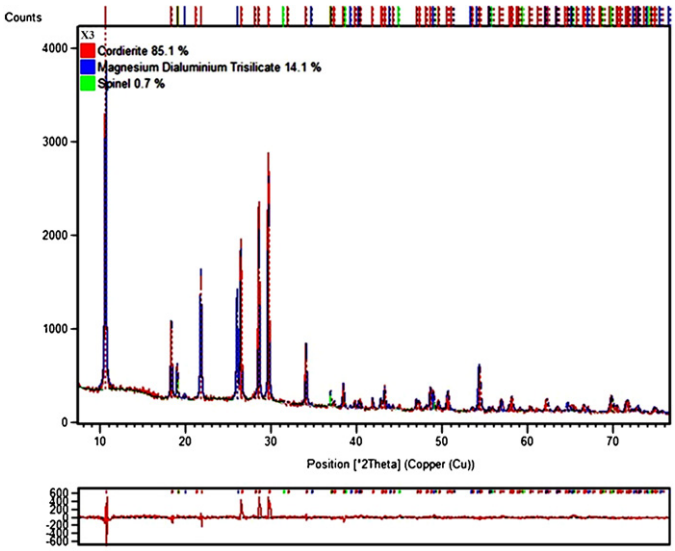

Fig. 11. Rietveld plot of sample X3.

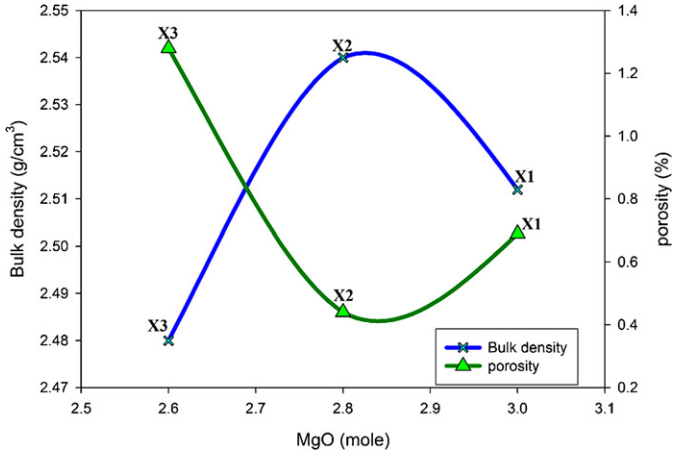

Fig. 12. Bulk density and porosity for series of $xMgO{\cdot}1.5Al_2O_3{\cdot}5SiO_2$ samples.

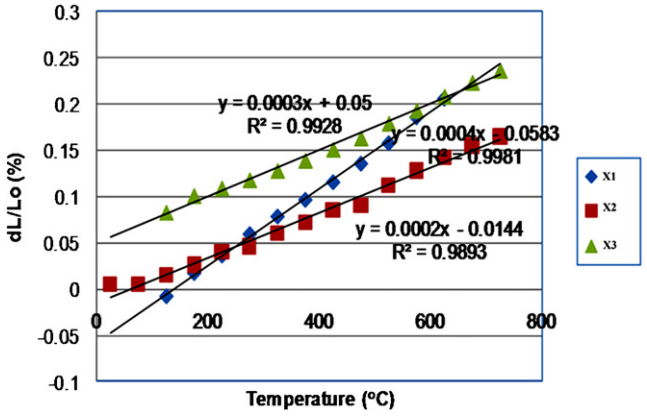

Fig. 13. Proportion line for calculating coefficient of thermal expansion of sintered rectangular pellets of samples X1, X2, and X3.

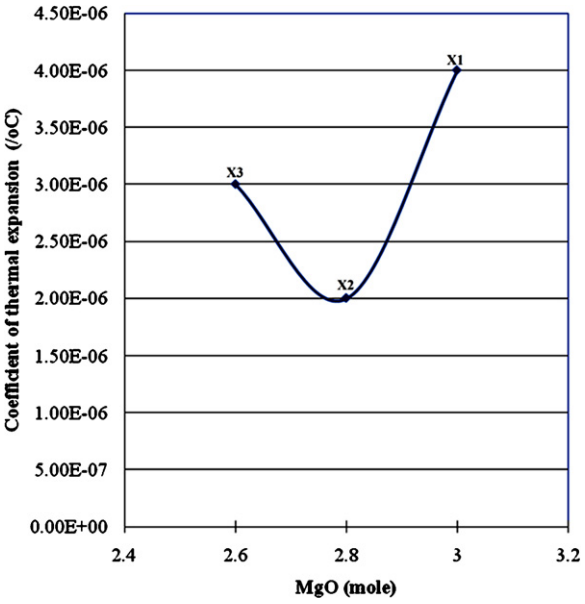

Fig. 14. Coefficient of thermal expansion of samples X1, X2 and X3.

still present in sample X1. The existence of multi crystalline phase with different crystal structures in the sample caused part of the space between the crystal to be arranged disorderly.

It is obvious that without any sintering aids, excess MgO up to 2.6 mol was not sufficient to retard the formation of μ-cordierite,

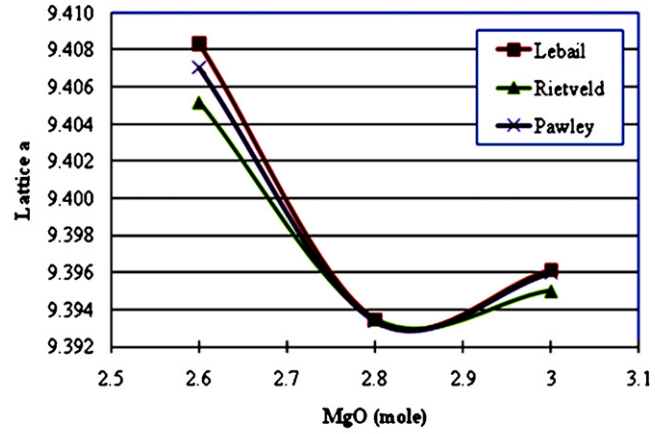

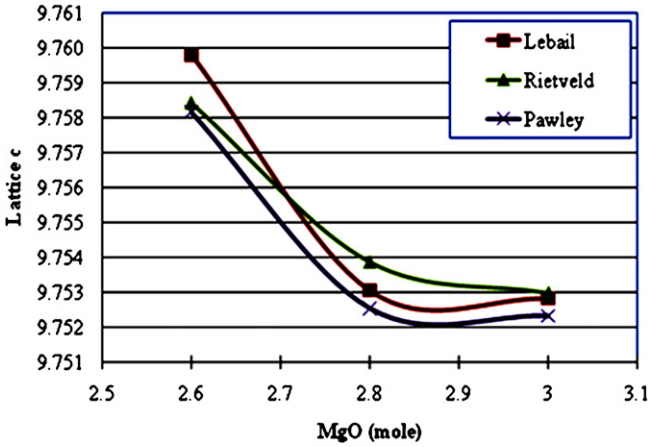

Fig. 15. Lattice changes as a function of MgO concentration ratio. (a) Lattice *a* and (b) lattice *c*.

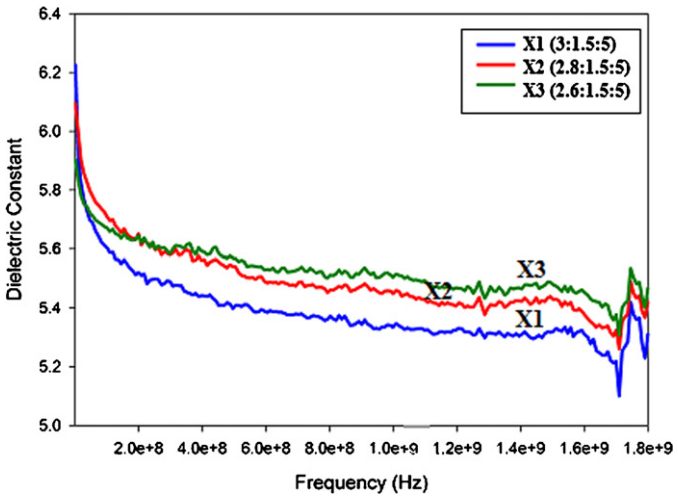

Fig. 16. Dielectric constant of samples as a function of frequency.

while at and/or above 3 mol MgO will result in the formation of a forsterite phase. Therefore, samples should be formulated with approximately 2.8 mol MgO with less Al_2O_3 (1.5 mol) from the exact cordierite stoichiometric composition in order to obtain single phase α-cordierite.

3.6. Density and porosity test

Fig. 12 illustrates bulk density and percent of porosity of sintered pellet as a function of MgO concentration ratio. The trend of density plots as a function of MgO concentration ratio is the opposite to the trend of porosity. Sample X2 has the highest density and lowest percentage of porosity among the three samples. The formation of a secondary phase with different crystal structures limits the densification process and consequently produces samples with higher porosity and less bulk density.

The formation of more than one crystalline phase during the sintering process in samples X1 and X3 caused the kinetic process for the viscous flow to be quite slow and required much energy to complete the process. Therefore, samples X1 and X3 with 8.7 and 14.0 wt% secondary phases, respectively, have lower densification than sample X2 which has highest wt% of α-cordierite phase.

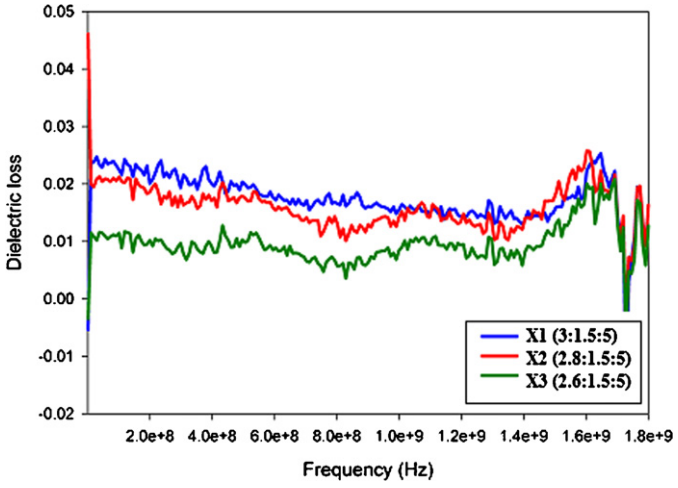

Fig. 17. Dielectric loss of samples as a function of frequency.

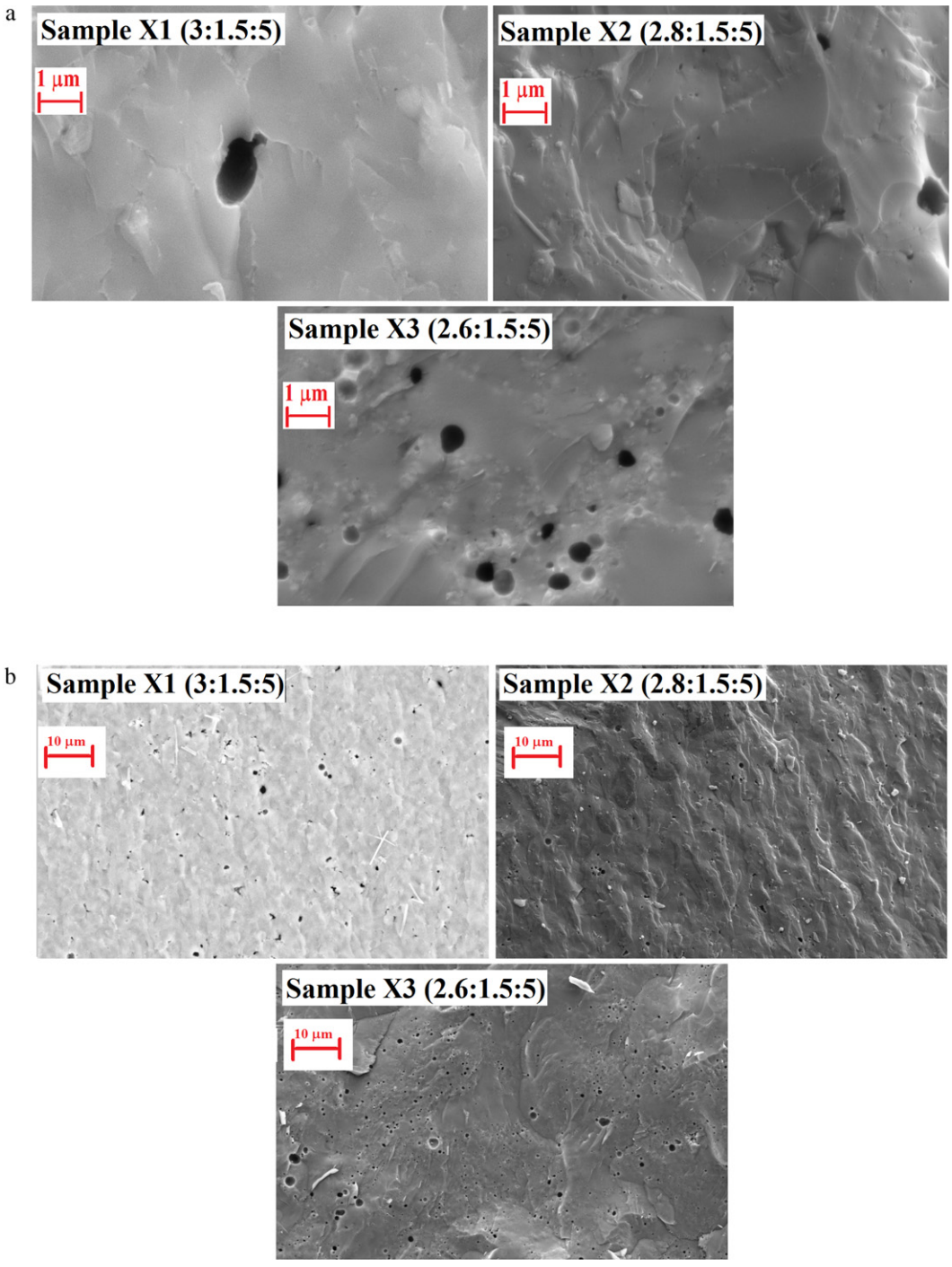

Fig. 18. (a) Microstructure of fracture surface at 10,000× magnification and (b) microstructure of fracture surface at 1000× magnification.

3.7. Coefficient of thermal expansion (CTE)

Thermal expansion was measured using sintered rectangular pellets in a dilatometry test machine. The CTE was calculated in the proportion region which is at temperature range 100–700 °C. Therefore, the curves of dL/Lo (%) vs *T* was replotted in a scatter diagram, as shown in Fig. 13, to obtain a linear equation. The slope value of the curves was divided by 100 to give the results of CTE. Results of CTE for samples with increasing levels of MgO are presented in Fig. 14. Most of the samples show low CTE, i.e. $2–4 \times 10^{-6}\,K^{-1}$. The low thermal expansion coefficient of the α-cordierite samples is the result of its relatively 'rigid' tetrahedral framework, and the anisotropic expansion of the octahedral framework of the α-cordierite structure. As shown in Fig. 14, CTE plots dropped from sample X1 to X2, and increased for sample X3. The decrease in CTE values for samples X1–X2 is associated to the increases of α-cordierite weight percentage as a function of MgO concentration. The existence of μ-cordierite, spinel and amorphous phase (Table 4) was responsible for the higher CTE in sample X3, while the increase in CTE values for sample X1 with 3.0 mol MgO may have resulted from the formation of a forsterite phase which has higher CTE. The crystallization process greatly altered the ther-

mal expansion of the glasses. Therefore, the glass-ceramic materials may have high or low coefficients of expansion depending on the expansion coefficients and elastic properties of the crystal phases formed [23].

In order to see the effect of increasing MgO in the crystal structure of α-cordierite, precise lattice parameters were determined from structure refinement using Lebail, Pawley and Rietveld methods using XRD software. A plot showing the effect of *a*- and *c*-lattice parameters with respect to increasing MgO concentration ratio is given in Fig. 15.

Sample X3 with composition $2.6MgO{\cdot}1.5Al_2O_3{\cdot}5SiO_2$ has the highest lattice *a* and lattice *c* values. The expansion of lattice *a* and lattice *c* was expected due to the existence of higher amounts of secondary phase inside α-cordierite crystals and finally expand the lattice *a* and lattice *c*. Volumes of unit cells for these secondary phases (forsterite 289.93×10^6 pm^3, μ-cordierite = 124.65×10^6 pm^3, spinel = 524.39×10^6 pm^3) are lower than those of the α-cordierite phase (771×10^6 pm^3). Therefore, some of the secondary phases could reside interstitially in between the α-cordierite crystals, producing a higher volume.

3.8. Dielectric properties

3.8.1. Dielectric constant

The dielectric constants of samples with different MgO concentration ratios are presented in Fig. 16 as a function of frequency from 1 MHz to 1 GHz. The dielectric constant decreased with increasing frequency from 1 MHz to 1 GHz for all samples. An increase in frequency induces weakening or disappearing of ionic polarization, and consequently decreases dielectric constant values. The dielectric constant of the samples with different MgO concentration ratios is in the range of 5.3–5.5, from a frequency of 1 MHz to 1 GHz. The values are in close agreement with other published values. Dielectric constant decreases with increasing MgO. Reduction in dielectric constant as a function of MgO in the series of $x MgO{\cdot}1.5Al_2O_3{\cdot}5SiO_2$ samples resulted from phase transformation and the amount of porosity in the sample. Although the percentage of porosity in sample X3 with 2.6 mol MgO is the highest among the three samples, it possesses high dielectric constant. The high dielectric constant in sample X3 may have resulted from high residual glass content in this sample. Samples with higher glassy or amorphous phase contain mobile ions. These mobile ions can jump between two sites in the open network structure of glasses, thus increasing the dielectric constant of the sample. Sample X1 has higher dielectric constant than sample X2 due to its higher porosity content. However, the difference is too small, and still within the standard range.

3.8.2. Dielectric loss

The dielectric loss as a function of frequency is presented in Fig. 17. Sample X1 with a higher percentage of porosity has the highest dielectric loss followed by samples X3 and X2. The dielectric loss of all samples is within 10^{-2} which is slightly higher compared to reported data which used pure oxides as a precursor in cordierite synthesis. α-Cordierite synthesized from pure oxide generally has very low dielectric loss $<10^{-3}$ at 10 MHz [14,24]. Higher concentrations of α-cordierite phase do not necessarily have low loss. The high values of dielectric loss in this study, compared to α-cordierite synthesized using pure oxide precursors, are caused by increased polarization due to defects in the structure and impurities or metal oxide at grain boundaries. Some oxides, especially those which have excessive electrical conductivity at elevated temperatures, cause dielectric losses in ceramic materials. Dielectric losses may also be caused by the dipole movement of polarized molecules in the electrical field or non-homogeneity of the structure.

3.9. FESEM/EDX analysis

Microstructure of fracture samples as demonstrated in Fig. 18(a) and (b) clearly shows that sample X2 is fully densified with the lowest porosity content, followed by samples X3 and X1. The observation of porosity from a microstructure analysis was in good agreement with porosity content measured by the Archimedes principle. Percentage of porosity significantly influenced the bulk density and dielectric property values of the samples.

4. Conclusions

All three non-stoichiometric cordierite samples with excess modifying oxide and less intermediate oxide can be melted at 1500 °C to obtain fully amorphous glass powder. The crystallization temperature decreased as a function of MgO. Although the softening temperature and temperature at which the samples stop shrinking are the same for all three samples, samples shrunk at different rates due to the variation in the viscosity of the glass. The sample with the highest MgO concentration has the highest shrinkage rate, and vice versa. Although sample X1 with the highest modifying oxide (MgO) was expected to have a better degree of densification, the crystallization of multi crystalline phase with different crystal structures in the sample caused percentage of porosity to increase. The presence of other crystalline phases caused intensity counts of α-cordierite peak of sample X1 to be lower than X2 even though sample X1 has the highest degree of crystallinity (measured from DTA curves). Coefficient of thermal expansion of samples depends on the type of crystalline phase which exists in the sample. The sample with the chemical formulation $2.8MgO{\cdot}1.5Al_2O_3{\cdot}5SiO_2$ possesses the lowest CTE compared to the other samples. The dielectric constant decreased with increasing MgO. However, its values were still within the standard range. The dielectric loss was slightly higher than α-cordierite synthesized from pure oxide due to the existence of impurities from the starting raw materials.

Acknowledgements

The authors gratefully acknowledge the financial support from Islamic Development Bank Saudi Arabia and Fundamental Research Grant Scheme (9003-00171) Universiti Malaysia Perlis, and technical assistants from Universiti Sains Malaysia (USM).

References

[1] S. Kurama, H. Kurama, Ceram. Int. 34 (2008) 269–272.
[2] E. Yalamac, S. Akkurt, Ceram. Int. 32 (2006) 825–832.
[3] R. Goren, H. Gocmez, C. Ozgur, Ceram. Int. 32 (2006) 407–409.
[4] R. Goren, C. Ozgur, H. Gocmez, Ceram. Int. 32 (2006) 53–56.
[5] C. Ghitulica, E. Andronescu, O. Nicola, A. Dicea, M. Birsan, J. Eur. Ceram. Soc. 27 (2007) 711–713.
[6] I. Jankovic-Castvan, S. Lazarevic, D. Tanaskovic, A. Orlovic, R. Petrovic, D. Janackovic, Ceram. Int. 33 (2007) 1263–1268.
[7] I. Jankovic-Castvan, S. Lazarevic, B. Jordovic, R. Petrovic, D. Tanaskovic, D. Janackovic, J. Eur. Ceram. Soc. 27 (2007) 3659–3661.
[8] M.K. Naskar, M. Chatterjee, J. Eur. Ceram. Soc. 24 (2004) 3499–3508.
[9] A.M. Menchi, A.N. Scian, Mater. Lett. 59 (2005) 2664–2667.
[10] Y. Hu, H.T. Tsai, Mater. Chem. Phys. 52 (1998) 184–188.
[11] J. Banjuraizah, H. Mohamad, Z.A. Ahmad, Int. J. Appl. Ceram. Technol. (2010), doi:10.1111/j.1744-7402.2010.02486.x.
[12] J. Banjuraizah, H. Mohamad, Z.A. Ahmad, J. Am. Ceram. Soc. (2010), doi:10.1111/j.1551-2916.2010.04144.x.
[13] P.W. McMillan, in: J.P. Roberts (Ed.), Glass–Ceramics. Crystallization and Devitrification, vol. 1, Academic Press Inc., London, 1969.
[14] B.H. Kim, K.H. Lee, J. Mater. Sci. 29 (1994) 6592–6598.
[15] T. Rudolph, W. Pannhorst, G. Petzow, J. Non-Cryst. Solids 144 (1993) 273–281.
[16] A. Goel, D.U. Tulyaganov, S. Agathopoulos, M.J. Ribeiro, J.M.F. Ferreira, Ceram. Int. 33 (2007) 1481–1487.
[17] G.-H. Chen, X.-Y. Liu, J. Alloys Compd. 431 (2007) 282–286.
[18] G.-H. Chen, J. Alloys Compd. 455 (2008) 298–302.

[19] J. Schmelzer, J. Möller, I. Gutzow, R. Pascova, R. Müller, W. Pannhorst, J. Non-Cryst. Solids 183 (1995) 215–233.
[20] S. Reinsch, M.L.F. Nascimento, R. Müller, E.D. Zanotto, J. Non-Cryst. Solids 354 (2008) 5386–5394.
[21] E.D. Zanotto, J. Non-Cryst. Solids 129 (1991) 183–190.
[22] M. Dittmer, M. Müller, C. Rüssel, Mater. Chem. Phys. 124 (2010) 1083–1088.
[23] S.M. Salman, H. Darwish, E.A. Mahdy, Mater. Chem. Phys. 112 (2008) 945–953.
[24] S. Wang, H. Zhou, L. Luo, Mater. Res. Bull. 38 (2003) 1367–1374.